

## RELATIVISTIC MEASUREMENTS FROM TIMING THE BINARY PULSAR PSR B1913+16

J. M. WEISBERG AND Y. HUANG

Department of Physics and Astronomy, Carleton College, Northfield, MN 55057

*Draft version June 10, 2016*

### ABSTRACT

We present relativistic analyses of 9257 measurements of times-of-arrival from the first binary pulsar, PSR B1913+16, acquired over the last thirty-five years. The determination of the “Keplerian” orbital elements plus two relativistic terms completely characterizes the binary system, aside from an unknown rotation about the line of sight; leading to a determination of the masses of the pulsar and its companion:  $1.438 \pm 0.001 M_{\odot}$  and  $1.390 \pm 0.001 M_{\odot}$ , respectively. In addition, the complete system characterization allows the creation of tests of relativistic gravitation by comparing measured and predicted sizes of various relativistic phenomena. We find that the ratio of observed orbital period decrease due to gravitational wave damping (corrected by a kinematic term) to the general relativistic prediction, is  $0.9983 \pm 0.0016$ ; thereby confirming the existence and strength of gravitational radiation as predicted by general relativity. For the first time in this system, we have also successfully measured the two parameters characterizing the Shapiro gravitational propagation delay, and find that their values are consistent with general relativistic predictions. We have also measured for the first time in any system the relativistic shape correction to the elliptical orbit,  $\delta_{\theta}$ , although its intrinsic value is obscured by currently unquantified pulsar emission beam aberration. We have also marginally measured the time derivative of the projected semimajor axis, which, when improved in combination with beam aberration modelling from geodetic precession observations, should ultimately constrain the pulsar’s moment of inertia.

*Subject headings:* binaries: close — gravitation — gravitational waves — pulsars: individual (PSR B1913+16)

### 1. INTRODUCTION

Pulsar B1913+16 was the first binary pulsar discovered (Hulse & Taylor 1975). The system consists of two neutron stars (one an observed pulsar) orbiting in a very tight, highly eccentric orbit, and it remains one of the best for studying relativistic gravitation (Weisberg & Taylor 1981; Taylor & Weisberg 1982, 1989; and Weisberg, Nice, & Taylor 2010, hereafter WNT). In this paper, we update WNT with the addition of post-2006 data and with further relativistic timing analyses. The addition of significant quantities of data acquired with modern data-acquisition devices has enabled us to measure several additional relativistic phenomena for the first time in this system, while also refining previously-measured ones. Among the parameters newly measured with various degrees of accuracy are the Shapiro gravitational propagation delay, a relativistic correction to the elliptical orbital shape, and the time derivative of projected pulsar semimajor axis. All of the the data used in this study are published with this paper, while our analysis software is published in an online repository.

We describe the observations used in this work in §2, while §3 delineates the scope and methods of our relativistic analyses of these data. The results of our fits to the data are explained in §4, and their applications for tests of relativistic gravitation are discussed in §5. We conclude in §6 by summarizing our work and placing it in the context of results from other relativistic binary pulsar systems.

### 2. DATA

The data for our analyses consists of 9257 pulse times of arrival (TOAs) derived from five-minute integrations of the pulsar signal at frequencies near 1400 MHz measured at Arecibo Observatory from 1981 - 2012. The parameters of the various observing systems and the number of TOAs from each through epoch 2006 are tabulated in WNT; WAPP spectrometer observations since then have added another 1652 TOAs to the total, each acquired by three WAPPs deployed simultaneously at approximately contiguous 100-MHz bands near 1400 MHz.

Geodetic precession of the pulsar spin axis has induced pulse profile changes (Weisberg et al. 1989; Kramer 1998; Weisberg & Taylor 2002; Clifton & Weisberg 2008) that have lately grown increasingly larger, presumably as our line of sight approaches the edge of the pulsar beam. Nevertheless, for purposes of uniformity, we use only a single profile template while finding TOAs for all WAPP data. This procedure induces time offsets into our TOA dataset between different sessions and frequencies, which have grown to a level where they should be compensated for. To do so, we adopted the following process. First, we formed a pulse profile at each frequency band for each two-week session. Each resulting “session - band” standard profile has much greater  $S/N$  than does a single five - minute integration, while still being short enough to avoid the secular changes we are trying to measure. Next, we measured the offset of the midpoint of this session - band standard profile with respect to the grand standard profile. (The midpoint is assumed to correspond to a fixed longitude on the pulsar regardless of

profile shifts).

Then we fitted out a “primary” linear model of the profile offsets as a function of time at each band. In this fashion, we provided an empirically determined, model independent, first-order TOA correction that accounts for the effects of profile changes, thereby minimizing the long-term effects of profile shifts that might be mistaken as the signature of other phenomena. We next fitted the timing model to all such “primarily-offsetted” TOAs and chose the resulting dispersion measure as our nominal value. Finally, secondary offsets were determined through single session fits, where the dispersion measure was fixed at its nominal value and the residual offset of each band was fitted for and then removed. This process ensures that the infinite-frequency TOAs calculated from each band and session are self-consistently de-dispersed<sup>1</sup> and offsetted.

To verify that the above profile-variation-correction process does not contaminate our parameter measurements, we also employed an alternate approach, fitting for an offset for each band in each session simultaneously with all other parameters (Demorest et al. 2013). This procedure yields parameters that agree with our method to within  $1\sigma$  for all parameters, suggesting that our measurements are robust with respect to the methods used to remove profile-shift-induced timing offsets.

### 3. RELATIVISTIC ANALYSIS OF TOAs

Using an augmented version of the TEMPO software program, we fitted the relativistic timing model of Damour & Deruelle (1986, hereafter DD); or, in certain cases, the DD model augmented by the Freire & Wex (2010, hereafter FW) Shapiro parametrization (see §3.1),<sup>2</sup> to our TOAs. In these models, the pulsar signal encounters several distinct types of delays on its journey from the orbiting pulsar to the solar system barycenter, such that the infinite-frequency pulse arrival time at the solar system barycenter,  $t_{\text{ssbc}}$ , is given by:

$$t_{\text{ssbc}} = D^{-1}[T + \Delta_{\text{Roemer}}(T) + \Delta_{\text{Einstein}}(T) + \Delta_{\text{Shapiro}}(T) + \Delta_{\text{Aberration}}(T)]; \quad (1)$$

where each delay is a function of the pulsar proper time of pulse emission,  $T$ , and whose details depend on a number of physical parameters that are fitted for. (The Doppler factor  $D$  accounts for the relative motion of the solar system and binary system barycenters.) The various terms in Eq. 1 are detailed in DD and Damour & Taylor (1992, hereafter DT92), and we will comment further on the last two terms of Eq. 1 in the following two sections.

Among the fitted parameters, we determined improved values of the pulsar spin and orbital parameters that were published in WNT, plus a number of new ones. For the first time, we have successfully fitted for the Shapiro (1964) gravitational propagation delay while also placing constraints on two additional ones: a relativistic correction to the quasi-elliptical shape of the orbit and the

shrinkage rate of its projected semimajor axis, as described further below.

The improved, previously fitted parameters include the pulsar spin frequency and derivative(s)  $f$ ,  $\dot{f}$ , ...; five “Keplerian” orbital elements defined as projected pulsar semimajor axis  $x \equiv a_1 \sin i$  where  $i$  is the orbital inclination, orbital period  $P_b$ , eccentricity  $e$ , reference epoch  $T_0$ , the reference epoch’s longitude of periastron  $\omega_0$ ; relativistic “post-Keplerian” parameters defined as mean rate of periastron advance  $\langle \dot{\omega} \rangle$ , gravitational redshift - time dilation term  $\gamma$ , and orbital period derivative  $\dot{P}_b$ .

The newly fitted post-Keplerian parameters include the following: (i) two Shapiro delay terms called shape  $s$  and range  $r$  in the DD parametrization, or two (different) quantities  $\varsigma$  and  $h_3$  in the alternate FW parametrization; (ii) the orbital elliptical shape correction parameter  $\delta_\theta^{\text{obs}}$  (to our knowledge never previously fitted for in any binary system), which appears in DT92’s full expression for Eq. 1’s Roemer term<sup>3</sup>; and (iii)  $\dot{x}^{\text{obs}}$  and  $\dot{e}^{\text{obs}}$ , the observed time derivatives of  $x$  and  $e$ . All of the new parameters are discussed in greater detail in §3.1-§3.3; while the fit results for both old and new parameters are described in §4, and relativistic tests resulting from these measurements are discussed in §5. A set of TEMPO input files containing input parameters and the TOAs is available as an online companion to this paper, on arXiv, and at zenodo: <http://dx.doi.org/10.5281/zenodo.54764>.

#### 3.1. Fitting for the Shapiro Gravitational Propagation Delay via two Different Parametrizations

Until this work, we have been unable to explicitly measure the two Shapiro gravitational propagation delay terms that characterize Eq. 1’s  $\Delta_{\text{Shapiro}}(T)$ , owing to their relatively small timing signature and to their covariance. The two terms are identified as  $s$  and  $r$  in DD; while FW recently developed an alternate parametrization of the phenomenon, wherein their two fitted parameters,  $\varsigma$  and  $h_3$ , are orthonormal. Our software implementation of their parametrization for high-eccentricity pulsars is available in our augmented version of TEMPO.<sup>2</sup>

The measurements of either pair of Shapiro parameters,  $(s, r)$  or  $(\varsigma, h_3)$ , can be utilized in either of two different manners, as described below.

First, if general relativity is assumed to be the correct theory of gravitation, then either pair of Shapiro measurables can be utilized as independent constraints on the orbital inclination and binary companion mass. We summarize the theory here, and then apply it in §4.2.

In the DD formulation,  $s$  and  $r$  translate directly into  $\sin i$  and  $m_2$  (the companion mass), respectively:

$$\sin i = s, \quad (2)$$

and

$$m_2 = \left(\frac{c^3}{G}\right) r = \left(\frac{r}{T_\odot}\right) M_\odot, \quad (3)$$

with  $c$  the speed of light,  $G$  the Newtonian gravitational constant,  $T_\odot = G M_\odot / c^3 = 4.925\,490\,947 \mu\text{s}$ .

<sup>3</sup> Before it can be utilized for tests of relativity, the  $\delta_\theta^{\text{obs}}$  parameter must be corrected for a comparable aberration term which is currently undeterminable (see §4.4).

<sup>1</sup> This procedure also absorbs TOA variations induced by DM fluctuations at the levels and timescales expected from studies of millisecond pulsars (You et al. 2007).

<sup>2</sup> See <http://sourceforge.net/projects/TEMPO/> for our augmented version of TEMPO, which contains our fitting routine for the FW Shapiro parameters in high-eccentricity binaries.

The alternate FW parametrization of the Shapiro delay gives

$$\sin i = \frac{2\zeta}{\zeta^2 + 1}, \quad (4)$$

while  $m_2$  is a combination of the two measurables ( $h_3, \zeta$ ):

$$m_2 = \left(\frac{c^3}{2G}\right) \frac{h_3}{\zeta^3} = \left(\frac{h_3/\zeta^3}{T_\odot}\right) M_\odot. \quad (5)$$

Alternatively, each measured parameter of the Shapiro pair can be considered to be an independent test of relativistic gravitation. We apply this procedure in §5.2.

### 3.2. Determination of the Relativistic Orbital Shape Correction $\delta_\theta$ in the Presence of the Aberration Delay

In order to successfully measure the intrinsic value of  $\delta_\theta$ , which nominally quantifies a relativistic correction to the shape of the approximately elliptical orbit in Eq. 1's Roemer delay expression, one must compensate the observed value for the influence of a phenomenon that comparably affects TOAs, namely the orbital-phase dependent aberration of the pulsar beam, as described by DD and DT92. Those authors provide a prescription for calculating and eliminating the confounding aberration signature from the observed value of  $\delta_\theta$ , if the aberration geometry is known. In principle, the necessary information can be gleaned from studies of profile changes resulting from geodetic precession of the pulsar spin axis (Weisberg & Taylor 2002; Clifton & Weisberg 2008). In this section, we summarize the theoretical expressions required to quantify  $\delta_\theta$  and aberration, and we will apply our observations to these results in §4.4.

The time delay  $\Delta_{\text{Aberration}}$  in Eq. 1, resulting from aberration of the rotating pulsar beam, is dependent on the time-variable transverse component of the pulsar's orbital velocity. DD and DT92 parametrize the instantaneous delay via the aberration parameters  $A(t)$  and  $B(t)$ :

$$\Delta_{\text{Aberration}} = A(t)\{\sin(\omega + A_e(u)) + e \sin \omega\} + B(t)\{\cos(\omega + A_e(u)) + e \cos \omega\}, \quad (6)$$

where  $A_e(u)$  is a true-anomaly-like quantity, and  $A(t)$  and  $B(t)$  are dependent on the precessing spin-axis geometry:

$$A(t) = -\frac{f^{-1}}{P_b} \frac{x}{\sin i (1 - e^2)^{1/2}} \frac{\sin \eta}{\sin \lambda}, \quad (7)$$

$$B(t) = -\frac{f^{-1}}{P_b} \frac{x}{\sin i (1 - e^2)^{1/2}} \frac{\cos i \cos \eta}{\sin \lambda}, \quad (8)$$

with  $\lambda$  and  $\eta$  the geodetically-precessing polar angles of the pulsar spin axis with respect to the line of sight and line of nodes, respectively. (DD and DT92 suggested the substitution of a single fixed parameter,  $A_0$ , for the two parameters  $A(t)$  and  $B(t)$ , because observations at the time suggested that the spin and orbital angular momenta are aligned. However, subsequent observations of pulse profile changes have shown that this is not the case.)

While the above equations provide a complete description of the calculation of  $\Delta_{\text{Aberration}}$  at any proper

emission time, DD and DT92 also provide an alternate approach that focuses on aberration parameters that change slowly (on precession timescales) as a result of spin-axis precession. This procedure, detailed below, is more closely tailored to parameters determinable from TOA analyses.

DT92 show that aberration will bias the observed value of the relativistic orbital shape parameter  $\delta_\theta^{\text{obs}}$  with respect to its intrinsic value  $\delta_\theta^{\text{intr}}$ :

$$\delta_\theta^{\text{obs}} = \delta_\theta^{\text{intr}} - \epsilon_A, \quad (9)$$

where the small parameter  $\epsilon_A$  is defined as

$$\epsilon_A \equiv \frac{A(t)}{x}. \quad (10)$$

Hence the observational bias can be removed, given measurements of the aberration parameter  $A(t)$  and the Keplerian quantity  $x$ . The corrected value  $\delta_\theta^{\text{intr}}$  could then serve as an additional test of gravitation theory.

### 3.3. Other Parameters Affected by the Aberration Delay

In addition to affecting  $\delta_\theta$ , DT92 show that aberration also affects the observed  $x$  and  $e$  values. However, the fractional corrections to  $x$  and  $e$  are tiny. More interesting is the effect of geodetic spin-axis precession on the time-derivatives of these parameters, because DT92 show that they are potentially measurable. The precessional motion will cause the aberration geometry to change, resulting in secular changes to  $A(t)$  and hence to  $\epsilon_A$  on precession timescales:

$$\frac{d\epsilon_A}{dt} = \frac{1}{x} \frac{dA(t)}{dt} = -\frac{f^{-1}}{P_b} \frac{1}{\sin i (1 - e^2)^{1/2}} \frac{\Omega_1^{\text{geodetic}}}{\sin^2 \lambda} \times (\sin i \cos \lambda \sin 2\eta + \cos i \sin \lambda \cos \eta), \quad (11)$$

where  $2\pi/\Omega_1^{\text{geodetic}}$  is the geodetic precession period of the pulsar spin axis. The observed, normalized time derivative of  $e$  results from the sum of two phenomena:

$$\left(\frac{\dot{e}}{e}\right)^{\text{obs}} = \frac{d\epsilon_A}{dt} + \left(\frac{\dot{e}}{e}\right)^{\text{GW}}, \quad (12)$$

where ‘‘GW’’ designates effects due to gravitational waves; while the observed, normalized time derivative of  $x$  stems from a combination of five terms:

$$\left(\frac{\dot{x}}{x}\right)^{\text{obs}} = \frac{d\epsilon_A}{dt} + \left(\frac{\dot{a}_1}{a_1}\right)^{\text{GW}} + \left(\cot i \frac{di}{dt}\right)^{\text{SO}} - \mu \cot i \sin(\Theta_\mu - \Omega) - \frac{\dot{D}}{D}, \quad (13)$$

where ‘‘SO’’ refers to spin-orbit coupling. (See Lorimer & Kramer (2004) for an expression that includes additional terms needed for some other binary pulsars.)

The quantity  $di/dt$  in the third term of Eq. 13, resulting from pulsar spin-orbit coupling, is developed here

from expressions in DT92:

$$\begin{aligned} \frac{di}{dt} &= \frac{G}{c^2} \left\{ 2 + \frac{3m_2}{2m_1} \right\} \frac{S_1}{a_R^3 (1-e^2)^{3/2}} \sin \lambda \cos \eta \\ &= \frac{1}{c^2} \left\{ 2 + \frac{3m_2}{2m_1} \right\} \frac{I_1 (2\pi f) (2\pi/P_b)^2}{(m_1 + m_2) (1-e^2)^{3/2}} \sin \lambda \cos \eta, \end{aligned} \quad (14)$$

where  $m_1$  is the pulsar mass,  $a_R$  is the semimajor axis of the relative orbit,  $S_1 = I_1(2\pi f)$  is the magnitude of the pulsar spin angular momentum, and  $I_1$  is its moment of inertia. The fourth term of Eq. 13 results from the changing projection of the line of sight onto the orbital plane due to proper motion, with  $\mu$  and  $\Theta_\mu$  respectively the amplitude and position angle of proper motion and  $\Omega$  the position angle of the line of nodes (Kopeikin 1996). The final term of Eq. 13, involving changes in the Doppler factor  $D$  of Eq. 1, is caused by the relative line-of-sight galactic accelerations of the solar system and the binary system.

The above equations demonstrate that measurements of  $\dot{e}$  or  $\dot{x}$ , along with experimental or theoretical determinations of some of the other quantities appearing therein, can usefully constrain yet others.

#### 4. RESULTS OF THE FITS

We fitted the parameters discussed above to the full set of TOAs, using the TEMPO software, as modified by us.<sup>1</sup> See Tables 1 and 2 for our results and their estimated uncertainties. The uncertainties quoted therein represent the standard errors from the TEMPO fit (except as noted). This convention differs from our previous practice, wherein many uncertainties were instead estimated from fitted parameter variations across multiple reasonable fits. While the old procedure facilitated the incorporation of some systematic uncertainties into the error budget; the more stable recent instrumental configurations appear to minimize such effects.

Some of the fitted parameters shifted by several  $\sigma$  with respect to the values reported in Weisberg et al. (2010). The shifts can all be attributed to the new incorporation of a frequency and time offset for each WAPP observing session and center frequency in order to account for geodetic-precession-induced profile changes (see §2), and to our new procedure of fitting for rather than freezing at 0 the parameter  $\dot{x}$ . The latter procedure also led to a significantly larger uncertainty in the fitted value of  $\gamma$  and in quantities derived therefrom.

The astrometric and spin solutions are listed in Table 1. These are quite similar to those given in Weisberg et al. (2010), except that our longer post-glitch baseline made it clear that the previously discovered glitch at MJD  $\approx 52770$  is better modeled with the addition of a change in spin frequency *derivative*,  $\Delta\dot{f}$ . There remains only one known glitch having a significantly smaller value of  $\Delta f/f$  [in globular cluster millisecond PSR B1821-24 (Mandal et al. 2009)], although several of magnitude similar to the one tabulated here are now known. [See the online Jodrell Bank Pulsar Glitch Catalogue<sup>4</sup> (Espinoza et al 2011)]. Note that, as with Weisberg et al. (2010), ten higher-order spin derivatives were also fitted for to

**Table 1**  
Astrometric and Spin Parameters

Parameter	Value <sup>a</sup>
$t_0$ (MJD) <sup>b</sup> .....	52984.0
$\alpha$ (J2000) .....	19 <sup>h</sup> 15 <sup>m</sup> 27 <sup>s</sup> .99942(3)
$\delta$ (J2000) .....	16°06'27".3868(5)
$\mu_\alpha$ (mas yr <sup>-1</sup> ) .....	-1.23(4)
$\mu_\delta$ (mas yr <sup>-1</sup> ) .....	-0.83(4)
$f$ (s <sup>-1</sup> ) .....	16.940537785677(3)
$\dot{f}$ (s <sup>-2</sup> ) .....	-2.4733(1) $\times 10^{-15}$
Glitch Parameters	
Glitch epoch (MJD)...	52777(2)
$\Delta f$ (s <sup>-1</sup> ) .....	5.49(3) $\times 10^{-10}$
$\Delta\dot{f}$ (s <sup>-2</sup> ) .....	-2.7(1) $\times 10^{-18}$

<sup>a</sup> Figures in parentheses represent formal TEMPO standard errors in the last quoted digit, except for the glitch parameters. The stated uncertainty in glitch epoch results from empirically varying the glitch epoch until  $\Delta\chi^2$  corresponds to the 68% confidence level; the quoted uncertainties in the other glitch parameters were derived from their variations as the glitch epoch was varied over the chosen range.

<sup>b</sup> This quantity is the epoch of the next six measurements tabulated here.

**Table 2**  
Orbital Parameters

Parameter	Value <sup>a</sup>
$T_0$ (MJD) .....	52144.90097849(3)
$x \equiv a_1 \sin i$ (s)...	2.341776(2)
$e$ .....	0.6171340(4)
$P_b$ (d) .....	0.322997448918(3)
$\omega_0$ (deg) .....	292.54450(8)
$\langle \dot{\omega} \rangle$ (deg / yr)...	4.226585(4)
$\gamma$ (ms) .....	0.004307(4)
$P_b^{obs}$ .....	-2.423(1) $\times 10^{-12}$
$\delta_\theta^{obs}$ .....	4.0(25) $\times 10^{-6}$
$\dot{x}^{obs}$ .....	-0.014(9) $\times 10^{-12}$
$\dot{e}^{obs}$ (s <sup>-1</sup> ) .....	0.0006(7) $\times 10^{-12}$

#### Shapiro Gravitational Propagation Delay Parameters

##### Damour & Deruelle (1986) Parametrization

$s$ .....	0.68 <sup>+0.10</sup> <sub>-0.06</sub>
$r$ ( $\mu$ s) .....	9.6 <sup>+2.7</sup> <sub>-3.5</sub>

##### Freire & Wex (2010) Parametrization

$\varsigma$ .....	0.38(4)
$h_3$ .....	0.6(1) $\times 10^{-6}$

<sup>a</sup> Figures in parentheses represent formal TEMPO standard errors in the last quoted digit. The DD Shapiro parameters  $s$  and  $r$ , which are highly covariant, and their uncertainties, were refined through a process illustrated in Fig. 2.

eliminate the effects of timing noise. Their values are not shown in the Table as they do not correspond to meaningful physical parameters.

Table 2 displays the results of our fit to orbital parameters, including the eight final entries, which are fitted here for the first time in this system. Note that the first

<sup>4</sup> <http://www.jb.man.ac.uk/pulsar/glitches.html>

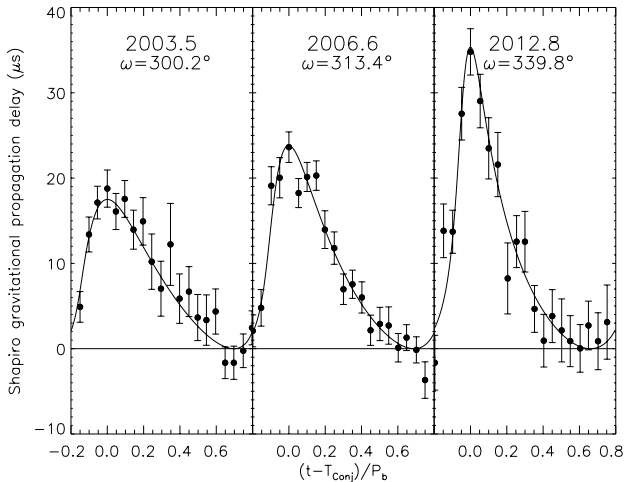


**Figure 1.** The Shapiro gravitational propagation delay variation around the orbit at three epochs. The curve represents the expected delay based on a general relativistic calculation, while the points and their error bars result from combining all residuals to a special fit (see text) near the given epoch into one of 20 orbital time bins. Time is reckoned with respect to  $T_{\text{Conj}}$ , the epoch of the pulsar’s superior conjunction with the companion. Each curve peaks at that epoch, when the pulsar’s earthbound signals plunge most deeply into the companion’s gravitational well. The amplitude and shape of the curves evolve, due to relativistic precession of the orbital ellipse, as quantified by the advancing longitude of periastron  $\omega$ .

two of these eight new parameters, namely  $\delta_\theta^{\text{obs}}$  and  $\dot{x}^{\text{obs}}$ , are measured at the marginal  $1.5\sigma$  level, while the third,  $\dot{e}^{\text{obs}}$ , is only an upper limit. All others in this Table, including the new Shapiro terms, are measured with high confidence. In the next sections, we discuss important orbital measurables, including corrections that must be made to some of the observed quantities in order to determine their intrinsic values.

#### 4.1. The Observed and Intrinsic Orbital Period Derivative

The observed orbital period derivative  $\dot{P}_b^{\text{obs}}$ , must be corrected by a term  $\dot{P}_b^{\text{gal}}$ , resulting from the relative galactic accelerations of the solar system and the binary system (Damour & Taylor [1991, hereafter DT91], DT92), in order to yield the intrinsic derivative,  $\dot{P}_b^{\text{intr}}$ :

$$\dot{P}_b^{\text{intr}} = \dot{P}_b^{\text{obs}} - \dot{P}_b^{\text{gal}}. \quad (15)$$

Using galactic parameters of  $R_0 = 8.34 \pm 0.16$  kpc and  $\Theta_0 = 240 \pm 8$  km/s from Reid et al. (2014), a pulsar distance estimate from Weisberg et al. (2008), and the pulsar proper motion from Table 1, we find that  $\dot{P}_b^{\text{gal}} = -(0.025 \pm 0.004) \times 10^{-12}$ . Inserting also  $\dot{P}_b^{\text{obs}}$  from Table 2 into Eq. 15, we calculate that  $\dot{P}_b^{\text{intr}} = -(2.398 \pm 0.004) \times 10^{-12}$ . The uncertainty in this result is dominated by the error in  $\dot{P}_b^{\text{gal}}$ , which in turn is set principally by the pulsar distance uncertainty. A VLBA parallax campaign on the pulsar, currently in progress, will hopefully improve these uncertainties.

#### 4.2. First Successful Measurement of the Shapiro Gravitational Propagation Delay Parameters in PSR B1913+16

Because of relativistic precession of the elliptical orbit, the Shapiro delay has recently grown to an amplitude of  $\sim 35 \mu\text{s}$  around the orbit, rendering it relatively easily measurable. Fig. 1 illustrates the enhancement of the Shapiro delay signal around the orbit over the last dozen years, during which time the WAPP receivers also came into use, thereby increasing our observing bandwidth ten-fold. The curves in the Figure illustrate a general relativistic calculation of the expected Shapiro delay variation around the orbit, while the data points are residuals to a TEMPO fit freezing all parameters at their best-fit values, except for the Shapiro parameter  $r$  (corresponding in General Relativity to the companion mass). The latter quantity was artificially set to zero to simulate the absence of the Shapiro delay in the fit. The pattern of residuals systematically matches theoretical expectations for the Shapiro delay.

We have now successfully determined the two Shapiro terms in both the DD and FW parametrizations (see Table 2). While the Shapiro delay has been observed in several other binary pulsar systems, these results mark the first successful detection of a pair of Shapiro measurables in the PSR B1913+16 system. [The two DD parameters,  $s$  and  $r$ , had been *jointly* constrained by Taylor & Weisberg (1989). For the ensuing decade, unfavorable orbital geometry rendered its amplitude unmeasurably small; while the last decade has seen both improving orbital geometry and advances in observing instrumentation.] We accounted for the significant nonlinear covariance of the the  $s$  and  $r$  parameters in estimating their values and uncertainties in Table 2, using a process delineated by Splaver et al. (2002). The procedure is illustrated graphically in Fig. 2, which also shows the best-fitting FW Shapiro parameters. (Tighter constraints on the inclination and companion mass can be derived *indirectly* from other measurements. See §4.3.)

#### 4.3. Best Determination of Component Masses and Orbital Inclination

The measurement of the first seven quantities in Table 2 enables the precise general relativistic determination of the component masses and orbital inclination. Specifically, our measurements of  $\langle \dot{\omega} \rangle$  and  $\gamma$ , along with the Keplerian elements, leave only the two unknowns  $m_{1;\langle \dot{\omega} \rangle, \gamma}$  and  $m_{2;\langle \dot{\omega} \rangle, \gamma}$  in the following two general relativistic equations:

$$\begin{aligned} \langle \dot{\omega} \rangle &= \\ &= 3 G^{2/3} c^{-2} (P_b/2\pi)^{-5/3} (1 - e^2)^{-1} (m_{1;\langle \dot{\omega} \rangle, \gamma} + m_{2;\langle \dot{\omega} \rangle, \gamma})^{2/3} \\ &= 3 T_\odot^{2/3} (P_b/2\pi)^{-5/3} (1 - e^2)^{-1} \left( \frac{m_{1;\langle \dot{\omega} \rangle, \gamma} + m_{2;\langle \dot{\omega} \rangle, \gamma}}{M_\odot} \right)^{2/3}, \end{aligned} \quad (16)$$

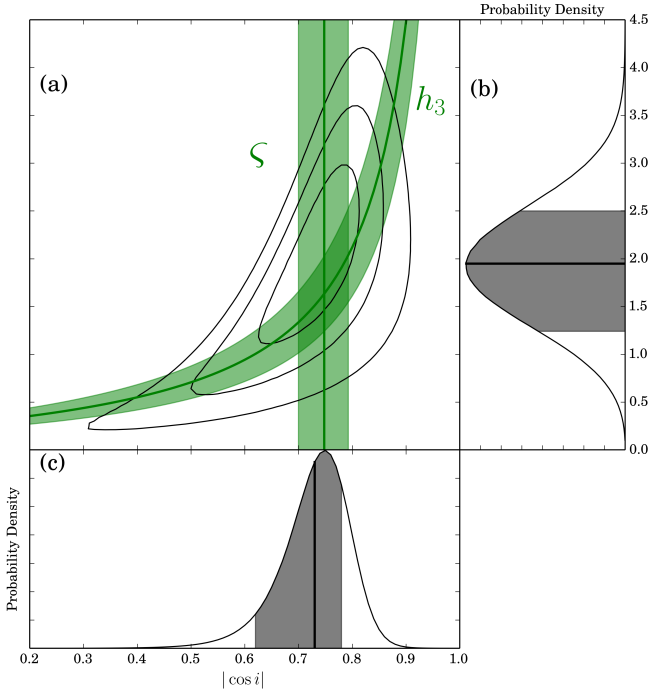


**Figure 2.** (a) Measured constraints on  $|\cos i|$  and  $m_2$  resulting from TEMPO fits for two different parametrizations of the Shapiro gravitational propagation delay within the context of general relativity. The Damour & Deruelle (1986)  $s$  and  $r$  parameters map directly onto the displayed  $|\cos i| [= +\sqrt{1-s^2}]$  and  $m_2 [= (r/T_\odot)M_\odot]$  axes, respectively; the black contours show joint 1, 2, and  $3\sigma$  ( $\Delta\chi^2 = 2.3, 6.2, 11.8$ ) confidence limits on those quantities, derived from a set of TEMPO fits to a large grid of (fixed)  $(|\cos i|, m_2)$ . The alternate Freire & Wex (2010) best-fit parameter constraints and their  $\pm 1\sigma$  limits are shown in green. Their fitted parameter  $\zeta$  transforms directly into the displayed  $|\cos i|$  axis (see Eq. 4), whereas their  $h_3$  parameter does not map uniquely onto either of the axes (see Eq. 5). The marginal distributions in (b) and (c) result from collapsing the resulting two-dimensional DD probability distribution onto the  $|\cos i|$  and  $m_2$  axes respectively, in which the mean (solid black) and the  $1\sigma$  bounds (grey region) are displayed, yielding  $|\cos i| = 0.73$  ( $+0.05, -0.11$ ) and  $m_2 = 1.95$  ( $+0.55, -0.71$ )  $M_\odot$  (68.3% confidence).

and

$$\begin{aligned} \gamma &= G^{2/3} c^{-2} e (P_b/2\pi)^{1/3} m_{2;\langle\dot{\omega}\rangle,\gamma} (m_{1;\langle\dot{\omega}\rangle,\gamma} + 2m_{2;\langle\dot{\omega}\rangle,\gamma}) \times \\ &\quad (m_{1;\langle\dot{\omega}\rangle,\gamma} + m_{2;\langle\dot{\omega}\rangle,\gamma})^{-4/3} \\ &= T_\odot^{2/3} e (P_b/2\pi)^{1/3} \frac{m_{2;\langle\dot{\omega}\rangle,\gamma}}{M_\odot} \times \\ &\quad \left( \frac{m_{1;\langle\dot{\omega}\rangle,\gamma} + 2m_{2;\langle\dot{\omega}\rangle,\gamma}}{M_\odot} \right) \left( \frac{m_{1;\langle\dot{\omega}\rangle,\gamma} + m_{2;\langle\dot{\omega}\rangle,\gamma}}{M_\odot} \right)^{-4/3} \end{aligned} \quad (17)$$

Solving simultaneously for the two component masses, we find that  $m_{1;\langle\dot{\omega}\rangle,\gamma} = 1.438 \pm 0.001 M_\odot$  and  $m_{2;\langle\dot{\omega}\rangle,\gamma} = 1.390 \pm 0.001 M_\odot$ . These values agree with WNT to within  $2\sigma$ , while our precision is poorer due to a less-precisely determined  $\gamma$  (see §4). Furthermore, Newtonian physics then yields an additional quantity from the derived masses and our  $x$  and  $P_b$  measure-

ments:  $(\sin i)_{\langle\dot{\omega}\rangle,\gamma} = 0.7327 \pm 0.0004$  (or, equivalently,  $|\cos i|_{\langle\dot{\omega}\rangle,\gamma} = 0.6806 \pm 0.0004$ ). These values are presently much more precise than the  $m_2$  and  $\sin i$  or  $|\cos i|$  values determined directly from the Shapiro propagation delay measurements of §4.2.

#### 4.4. Toward the First Published Measurement of the Relativistic Orbital Shape Correction, $\delta_\theta$ , in any System

We have successfully measured the apparent post-Keplerian orbital shape correction term,  $\delta_\theta^{\text{obs}}$  (see Table 2). As noted in §3.2, this observed value must be corrected for a comparable aberration signal  $\epsilon_A$  (see Eq. 9). Geodetic spin-precession modeling of this system should in principle determine the necessary aberration parameters by specifying the spin axis orientation (specifically, its polar angles  $\eta$  and  $\lambda$ ) over time (see Eq. 7). However, we find that the currently available pulseshape variation fits (Kramer 1998; Weisberg & Taylor 2002; Clifton & Weisberg 2008) yield inconsistent solutions for these parameters. Consequently, although we have successfully measured  $\delta_\theta^{\text{obs}}$ , it is not yet possible to determine  $\delta_\theta^{\text{intr}}$  nor hence to use its measured value as an additional test of relativistic gravitation.

Despite our current inability to measure  $\delta_\theta^{\text{intr}}$ , we can determine its *expected* value  $\delta_\theta^{\text{GR}}$  via a general relativistic calculation (DD; DT92):

$$\begin{aligned} \delta_\theta^{\text{GR}} &= \frac{G^{2/3}}{c^2} \left( \frac{P_b}{2\pi} \right)^{-2/3} (m_1 + m_2)^{-4/3} \left\{ \frac{7}{2} m_1^2 + 6m_1 m_2 + 2m_2^2 \right\} \\ &= T_\odot^{2/3} \left( \frac{P_b}{2\pi} \right)^{-2/3} \left( \frac{m_1 + m_2}{M_\odot} \right)^{-4/3} \times \\ &\quad \left\{ \frac{7}{2} \left( \frac{m_1}{M_\odot} \right)^2 + 6 \left( \frac{m_1 m_2}{M_\odot} \right) + 2 \left( \frac{m_2}{M_\odot} \right)^2 \right\}, \end{aligned} \quad (18)$$

yielding  $\delta_\theta^{\text{GR}} = (6.187 \pm 0.001) \times 10^{-6}$ . Eq. 9 can then be inverted to give the aberration parameter  $\epsilon_A = (2.2 \pm 2.5) \times 10^{-6}$ . This timing-derived value of  $\epsilon_A$  will provide a modest consistency check on future geodetic precession modeling.

#### 4.5. Implications of Fits for the First Time-Derivatives of $e$ and $x$

As noted above, Eqs. 12 and 13 demonstrate that the successful measurement of  $\dot{e}^{\text{obs}}$  and  $\dot{x}^{\text{obs}}$  would lead to constraints on other quantities of interest. It is therefore useful to further investigate the various terms composing these equations.

The first (aberration) term of both equations,  $d\epsilon_A/dt$ , was defined in Eqs. 10 and 11. However, as discussed in §4.4 for  $\epsilon_A$ , additional progress in understanding the pulsar's spin axis orientation is needed before  $d\epsilon_A/dt$  can be confidently determined. Nevertheless, our current geodetic precession modeling suggests that its value is in the  $\sim 10^{-15} \text{ s}^{-1}$  range, and varying with spin-precessional phase.

##### 4.5.1. Constraints from $\dot{e}^{\text{obs}}$

The second and final term of Eq. 12 involves the time evolution of  $e$  induced by gravitational wave (“GW”) emission. For the Eq. 12 second term, Peters (1964) shows that this term,

$$\begin{aligned} \left(\frac{\dot{e}}{e}\right)^{\text{GW}} &= -\frac{304}{15} \frac{G^3}{c^5 a_R^4} \mu (m_1 + m_2)^2 \times \\ &\quad (1 - e^2)^{-5/2} \left(1 + \frac{121}{304} e^2\right) \\ &= -\frac{304}{15} T_\odot^{5/3} \frac{\frac{m_1}{M_\odot} \frac{m_2}{M_\odot}}{(\frac{m_1+m_2}{M_\odot})^{1/3}} \left(\frac{P_b}{2\pi}\right)^{-8/3} \times \\ &\quad (1 - e^2)^{-5/2} \left(1 + \frac{121}{304} e^2\right) \\ &= -2.9 \times 10^{-17} \text{ s}^{-1}, \end{aligned} \quad (19)$$

with  $\mu$  the reduced mass. This term is negligible compared to the expected value of  $d\epsilon_A/dt$ , except at fortuitous precessional phases where the latter can drop to zero. Consequently, the  $d\epsilon_A/dt$  term dominates Eq. 12, so that a successful measurement of  $(\dot{e}/e)^{\text{obs}}$  would provide a unique measurement of  $d\epsilon_A/dt$ . Unfortunately, our fitted value of  $(\dot{e}/e)^{\text{obs}}$  is currently not significantly different from zero, although its upper limit is in the  $10^{-15} \text{ s}^{-1}$  range (see Table 2) expected for  $d\epsilon_A/dt$ .

#### 4.5.2. Constraints from $\dot{x}^{\text{obs}}$

The second term in Eq. 13 delineates the gravitational wave-induced orbital shrinkage rate, which can be evaluated from measurables via

$$\left(\frac{\dot{a}_1}{a_1}\right)^{\text{GW}} = \frac{2}{3} \left(\frac{\dot{P}_b}{P_b}\right)^{\text{GW}} = -5.7 \times 10^{-17} \text{ s}^{-1}. \quad (20)$$

The third (spin-orbit) term of Eq. 13 varies approximately sinusoidally on the geodetic precession timescale, with an amplitude of  $\sim \pm 3 \times 10^{-15} \text{ s}^{-1}$ . Details await a robust determination of geodetic precession parameters (see Eq. 14).

The fourth (Kopeikin 1996) term of Eq. 13 has a maximum amplitude<sup>5</sup> of  $\sim 2.3 \times 10^{-16} \text{ s}^{-1}$ ; while the fifth and final term,

$$-\frac{\dot{D}}{D} = +\frac{\dot{P}_{b, \text{gal}}}{P_b} = -1 \times 10^{-18} \text{ s}^{-1} \quad (21)$$

(see §4.1 for details on the calculation of  $\dot{P}_{b, \text{gal}}$ ).

In summary, the first (aberration) and third (spin-orbit) terms dominate Eq. 13, so all others may be ignored. However, neither of these two terms is currently accurately determinable. We do have a marginally significant measurement of  $\dot{x}^{\text{obs}}$  (see Table 2). Consequently, if either of the two terms becomes well-determined in the future along with an improved value of  $\dot{x}^{\text{obs}}$ , then the other term will also become accessible. For example, there are two possible paths toward determination of

the aberrational term: First, additional geodetic precession observations and modeling should better constrain  $d\epsilon_A/dt$ ; and second, additional observations could better determine  $\dot{e}^{\text{obs}}$ , which, as noted in §4.5.1, would then be equivalent to a measurement of  $d\epsilon_A/dt$ . At this point, the spin-orbit term would be calculable, leading to an exciting measurement of the pulsar’s moment of inertia, which has important implications for neutron star equations of state (Lattimer & Schutz 2005). With the measurement precision of  $\dot{x}$  and  $\dot{e}$  improving with time  $t$  as  $t^{-3/2}$ , another decade or so of observations are required. Unfortunately, geodetic spin axis precession may cause the pulsar to disappear before that time.

## 5. TESTS OF RELATIVISTIC GRAVITATION

The determination of seven particular independent quantities suffices to fully determine the dynamics of a binary system within the context of a particular theory of gravitation. For example, the most accurate determination of component masses and orbital inclination in §4.3 and of  $\delta_\theta^{\text{GR}}$  in §4.4 depend upon subsets of the first seven measurements listed in Table 2.

Consequently, any additional measurement constitutes an independent test of relativistic gravitation under strong-field conditions. In the following two sections, we delineate relativistic gravitational tests via measurements of gravitational radiation emission and of the Shapiro gravitational propagation delay, respectively.

### 5.1. Gravitational Radiation Emission and $\dot{P}_b$

Gravitational radiation emission should cause the orbit to decay as orbital energy is radiated away. The quantity  $\dot{P}_b^{\text{GR}}$  is the resulting orbital period derivative expected from a general relativistic calculation of this phenomenon (Peters and Mathews 1963):

$$\begin{aligned} \dot{P}_b^{\text{GR}} &= -\frac{192 \pi G^{5/3}}{5 c^5} \left(\frac{P_b}{2\pi}\right)^{-5/3} \left(1 + \frac{73}{24} e^2 + \frac{37}{96} e^4\right) (1 - e^2)^{-7/2} \\ &\quad \times m_1 m_2 (m_1 + m_2)^{-1/3} \\ &= -\frac{192 \pi}{5} T_\odot^{5/3} \left(\frac{P_b}{2\pi}\right)^{-5/3} \left(1 + \frac{73}{24} e^2 + \frac{37}{96} e^4\right) (1 - e^2)^{-7/2} \\ &\quad \times \left(\frac{m_1}{M_\odot}\right) \left(\frac{m_2}{M_\odot}\right) \left(\frac{m_1 + m_2}{M_\odot}\right)^{-1/3} \end{aligned} \quad (22)$$

Inserting our measured and derived values and their uncertainties into Eq. 22<sup>6</sup>, we find that  $\dot{P}_b^{\text{GR}} = (-2.40263 \pm 0.00005) \times 10^{-12}$ . To verify our estimate of the error in  $\dot{P}_b^{\text{GR}}$  that was derived via propagation of uncertainty, we also employed a Monte-Carlo method with Cholesky decomposition of the covariance matrix. In this fashion, we simulated the joint normal distribution of measured parameters  $\{\gamma, \dot{\omega}, P_b, e\}$ , and then constructed

<sup>5</sup> The exact value depends on the unknown alignment on the sky of the line of nodes.

<sup>6</sup> This value may also be calculated directly from the first seven orbital measurables in Table 2 alone, without the use of derived quantities such as the masses (DT91).

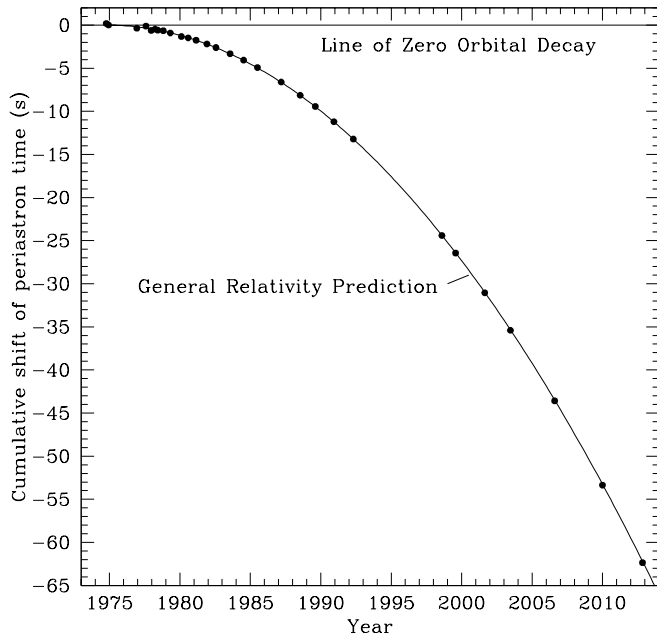


**Figure 3.** The orbital decay of PSR B1913+16 as a function of time. The curve represents the orbital phase shift expected from gravitational wave emission according to General Relativity. The points, with error bars too small to show, represent our measurements.

a histogram of 1000000 derived  $\dot{P}_b^{\text{GR}}$  and inferred the uncertainty therefrom.

Consequently, we find that

$$\frac{\dot{P}_b^{\text{intr}}}{\dot{P}_b^{\text{GR}}} = \frac{(-2.398 \pm 0.004) \times 10^{-12}}{(-2.40263 \pm 0.00005) \times 10^{-12}} = 0.9983 \pm 0.0016. \quad (23)$$

This result demonstrates that the system is losing energy to gravitational radiation within  $\sim 1\sigma$  of the rate predicted by general relativity (see also Fig. 3 and the red curve in Fig. 4). The above number represents a significant improvement over the value determined by WNT,  $0.997 \pm 0.002$ , which represented a  $1.8\sigma$  discrepancy between our measurements and general relativity. Interestingly, the new galactic parameters of Reid et al. (2014) are the principal reason for the improvement (via a change in  $\dot{P}_b^{\text{gal}}$ ), while our measured values themselves changed little.

In addition to confirming general relativistic radiation damping at this level, our result rules out large parameter spaces in plausible scalar-tensor theories of gravity. In recent years, however, other pulsars in neutron star-white dwarf binary systems have overtaken PSR B1913+16 in constraining these alternatives (Freire et al. 2012).

DD92 point out that this test is a “mixed” strong-field probe in that it involves a combination of radiative effects (via  $\dot{P}_b^{\text{obs}}$ ) and quasi-static phenomena (through  $\langle \dot{\omega} \rangle$  and  $\gamma$ , whose values are needed in order to make a prediction of the expected  $\dot{P}_b^{\text{GR}}$ ). Consequently, additional tests, such as those described in the next section, that probe different aspects of strong-field gravitation, are also useful in constraining viable alternatives to general relativity.

## 5.2. Shapiro Gravitational Propagation Delay

Each of the two newly measured Shapiro parameters represents another independent test of relativistic gravitation. As with the  $\dot{P}_b$  test of §5.1, the Shapiro tests also require the complementary measurement of  $\langle \dot{\omega} \rangle$  and  $\gamma$  in order to make a testable prediction for the value of the Shapiro parameters. In this case, unlike the  $\dot{P}_b$  test, all of the post-Keplerian quantities probe quasi-static phenomena in strong fields. While Shapiro parameters have already been measured in several other binary systems, it is especially useful to constrain theories via systems such as this one and PSRs B1534+12 and J0737-3039A, where at least three “excess” post-Keplerian parameters beyond  $\langle \dot{\omega} \rangle$  and  $\gamma$  (one gravitational radiation parameter and two Shapiro quantities) are measurable. Although the precision of the binary pulsar Shapiro parameter measurements is well below their measurement precision in the weak solar gravitational field, it is this simultaneous determination of several parameters in strong-field conditions in each of these binary pulsar systems that leads to the important constraints on relativistic theories of gravitation.

In the DD formulation of the Shapiro delay within general relativity, the Shapiro measurables  $s$  and  $r$  map directly onto  $\sin i$  and  $m_2$ , respectively. Hence we can test General Relativity by comparing the Shapiro determination of  $\sin i$  ( $\equiv s$ ) with that determined from  $\langle \dot{\omega} \rangle$  and  $\gamma$  (called  $\sin i_{\langle \dot{\omega}, \gamma} \equiv s$ ; see §4.3):

$$\frac{s}{\sin i_{\langle \dot{\omega}, \gamma}} = \frac{0.68^{+0.10}_{-0.06}}{0.7327 \pm 0.0004} = 0.93^{+0.14}_{-0.07}. \quad (24)$$

Similarly, we can test General relativity by comparing the Shapiro determination of  $m_2$  ( $\equiv r M_\odot / T_\odot$ ) with that determined from  $\langle \dot{\omega} \rangle$  and  $\gamma$ :

$$\frac{r M_\odot / T_\odot}{m_{2; \langle \dot{\omega}, \gamma}} = \frac{(1.95^{+0.55}_{-0.71}) M_\odot}{(1.390 \pm 0.001) M_\odot} = 1.40^{+0.40}_{-0.51}. \quad (25)$$

The consistency (albeit with a rather low level of precision) of these Shapiro determinations of  $\sin i$  and  $m_2$  with those measured via the other post-Keplerian terms, and hence their confirmation of general relativity, is also graphically depicted in Fig. 4. The Shapiro terms have also been measured in several other binary pulsar systems with higher precision, and have also been shown to be in agreement with general relativity.

## 6. CONCLUSIONS

We report here on the measurements and relativistic analyses of 9309 TOAs in over thirty years of high-quality Arecibo data on binary pulsar PSR B1913+16. We fitted for a number of previously unmeasurable parameters for the first time in this system (and in one case, for the first time anywhere), which enabled us to significantly advance our relativistic analyses of the system. We provide our newest measurements or derivations of all relevant physical quantities of the binary system, with the exception of  $\Omega$ , the position angle of the line of nodes. We rigorously ascertained the uncertainties in the fitted and derived parameters. Having fully characterized the system, we proceeded to use it in several tests of general relativity in strong-field conditions.

We have measured a gravitational radiation-induced

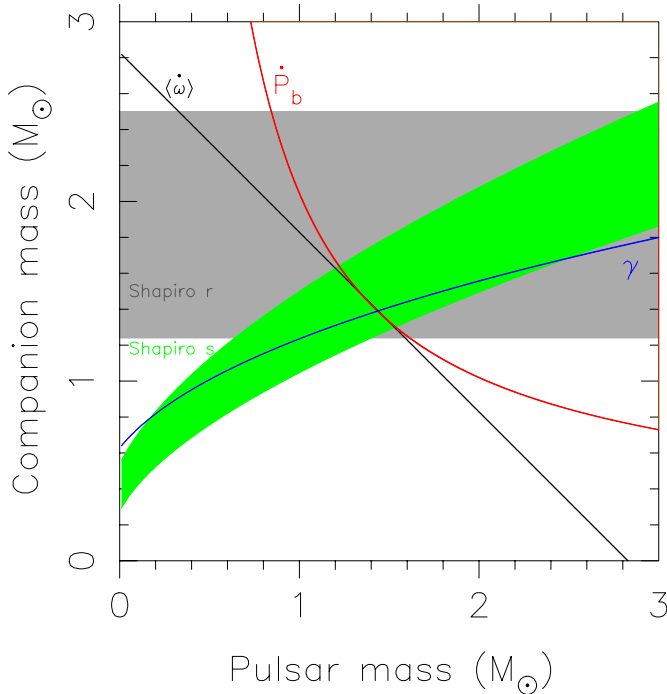


**Figure 4.** Constraints on the masses of the pulsar and the companion as a function of five post-Keplerian measurables, within the context of General Relativity. The width of each curve represents  $\pm 1\sigma$  error bounds. The mutual near-intersection of all curves illustrates the agreement of our observations with general relativity in the strong-field conditions at the binary system.

**Table 3**

Comparison of Gravitational Radiation-Induced Orbital Decay with GR Prediction in Binary Pulsars

PSR	$\dot{P}_b^{\text{intr}}/\dot{P}_b^{\text{GR}}$	Ref.
J0348+0432	$1.05 \pm 0.18$	Antoniadis et al. (2013)
J0737-3039	$1.003 \pm 0.014$	Kramer et al. (2006)
J1141-6545	$1.04 \pm 0.06$	Bhat, Bailes, & Verbiest (2008)
B1534+12	$0.91 \pm 0.06$	Stairs et al. (2002)
J1738+0333	$0.94 \pm 0.13$	Freire et al. (2012)
J1756-2251	$1.08 \pm 0.03$	Ferdman et al. (2014)
J1906+0746	$1.01 \pm 0.05^a$	van Leeuwen et al. (2015)
B1913+16	$0.9983 \pm 0.0016$	This work
B2127+11C	$1.00 \pm 0.03$	Jacoby et al. (2006)

<sup>a</sup> Assumes negligible proper motion.

orbital period decrease whose rate agrees with the general relativistic expectation to within  $\sim 1\sigma$ , which is closer than found by WNT, largely as a result of an improved galactic correction resulting from more accurate galactic parameters (Reid et al. 2014).

Similar orbital decay tests have now been performed with several other binary pulsars (see Table 3 for published measurements of  $\dot{P}_b^{\text{intr}}/\dot{P}_b^{\text{GR}}$ ). The orbital decays of PSRs J0348+0432, J0737-3039, J1141-4565, J1738+0333, J1906+0746, B1913+16, and B2127+11C all exhibit agreement between observation and general relativity to within (or very close to) the authors' stated uncertainties. PSR B1913+16 currently has the most precise such determination, and interferometric parallax measurements, currently in progress, will hopefully further tighten the precision.

Among the other two, PSR B1534+12 and PSR J1756-2251, various systematic effects such as an incorrect distance in the galactic acceleration correction may explain the small observed discrepancies, although it is possible that an incompleteness of general relativity or some unknown physical effect is responsible. See the work of Ferdman et al. (2014) for an especially thorough description of the most significant deviation of the orbital decay rate from the general relativistic prediction, found in PSR J1756-2251.

Our new (for this system) measurements of Shapiro gravitational propagation delay parameters represent two additional tests of relativistic gravitation, and are fully consistent with general relativity, although their relative precision is currently far lower than the orbital decay test. This binary now joins several other systems, including PSRs J0737-3039A, B1534+12, and J1756-2251, in each providing at least three independent tests of relativistic, strong-field gravitation.

We have also marginally measured the orbital shape parameter  $\delta_\theta$  for the first time anywhere, but its intrinsic value is corrupted by a comparable, undetermined aberration delay. Future geodetic spin-orbit precession measurements should lead to an accurate characterization of the aberration and then an additional relativistic gravitational test via the comparison of the aberration-corrected  $\delta_\theta^{\text{intr}}$  with  $\delta_\theta^{\text{GR}}$ .

In addition, we fitted for the time derivative of orbital eccentricity  $e$  and projected semimajor axis of the pulsar orbit,  $x$ , and we achieved an upper limit on the former and a marginal detection of the latter. We discussed and quantified the various physical phenomena that can contribute to these parameters. Unless the pulsar disappears in the next few years due to geodetic spin axis precession, future timing observations should better define these quantities, allowing for a determination of the pulsar's moment of inertia  $I_1$ .

We have placed online<sup>2</sup> a subroutine and modifications to the TEMPO TOA fitting software, which codes the Freire & Wex (2010) parametrization of the Shapiro delay for high-eccentricity binary pulsars such as the PSR B1913+16 system. An online companion of this paper provides the TEMPO input files and TOAs upon which these analyses are based. The same data are on arXiv, and at zenodo: <http://dx.doi.org/10.5281/zenodo.54764>.

Much of this experiment was pioneered by J. H. Taylor, to whom we owe our deepest thanks. D. J. Nice assisted with observing and analyses, and A. A. Chael assisted in developing the FW analysis package. The authors gratefully acknowledge financial support from the US National Science Foundation. The Arecibo Observatory is operated by SRI International under a cooperative agreement with the National Science Foundation (AST-1100968), and in alliance with Ana G. Mendez-Universidad Metropolitana, and the Universities Space Research Association.

*Facility:* Arecibo

## REFERENCES

Antoniadis, J., Freire, P. C. C., Wex, N., et al. 2013, *Science*, 340, 448

- Bhat, N. D. R., Bailes, M., & Verbiest, J. P. W. 2008, Phys. Rev. D, 77, 124017
- Clifton, T., & Weisberg, J. M. 2008, ApJ, 679, 687
- Damour, T. & Deruelle, N. 1986, Ann. Inst. H. Poincaré (Phys. Theorique), 44, 263 (DD)
- Damour, T., & Taylor, J. H. 1991, ApJ, 366, 501 (DT91)
- Damour, T., & Taylor, J. H. 1992, Phys. Rev. D, 45, 1840 (DT92)
- Demorest, P. B., Ferdman, R. D., Gonzalez, M. E., et al. 2013, ApJ, 762, 94
- Espinoza, C. M., Lyne, A. G., Stappers, B. W., & Kramer, M. 2011, MNRAS, 414, 1679
- Ferdman, R. D., Stairs, I. H., Kramer, M., et al. 2014, MNRAS, 443, 2183
- Freire, P. C. C., & Wex, N. 2010, MNRAS, 409, 199 (FW)
- Freire, P. C. C., Bassa, C. G., Wex, N., et al. 2011, MNRAS, 412, 2763
- Freire, P. C. C., Wex, N., Esposito-Farèse, G., et al. 2012, MNRAS, 423, 3328
- Hulse, R. A., & Taylor, J. H. 1975, ApJ, 195, L51
- Jacoby, B. A., Cameron, P. B., Jenet, F. A., et al. 2006, ApJ, 644, L113
- Kopeikin, S. M. 1996, ApJ, 467, L93
- Kramer, M. 1998, ApJ, 509, 856
- Kramer, M., Stairs, I. H., Manchester, R. N., et al. 2006, Science, 314, 97
- Lattimer, J. M., & Schutz, B. F. 2005, ApJ, 629, 979
- Lorimer, D. R., & Kramer, M. 2004, Handbook of pulsar astronomy. Cambridge observing handbooks for research astronomers, Vol. 4. Cambridge, UK: Cambridge University Press, p. 229
- Mandal, R. D. R., Konar, S., Dey, M., & Dey, J. 2009, MNRAS, 399, 822
- Peters. P. C., and Mathews, J. 1963, Phys Rev, 131, 435
- Peters. P. C. 1964, Phys Rev, 136, 1224
- Reid, M. J., Menten, K. M., Brunthaler, A., et al. 2014, ApJ, 783, 130
- Shapiro, I. I. 1964, Phys. Rev. Lett., 13, 789
- Splaver, E. M., Nice, D. J., Arzoumanian, Z., et al. 2002, ApJ, 581, 509
- Stairs, I. H., Thorsett, S. E., Taylor, J. H., & Wolszczan, A. 2002, ApJ, 581, 501
- Taylor, J. H., & Weisberg, J. M. 1982, ApJ, 253, 908
- Taylor, J. H., & Weisberg, J. M. 1989, ApJ, 345, 434
- van Leeuwen, J., Kasian, L., Stairs, I. H., et al. 2015, ApJ, 798, 118
- Weisberg, J. M., & Taylor, J. H. 1981, General Relativity and Gravitation, 13, 1
- Weisberg, J. M., Romani, R. W., & Taylor, J. H. 1989, ApJ, 347, 1030
- Weisberg, J. M., & Taylor, J. H. 2002, ApJ, 576, 942
- Weisberg, J. M., Stanimirović, S., Xilouris, K., Hedden, A., de la Fuente, A., Anderson, S. B., & Jenet, F. A. 2008, ApJ, 674, 286
- Weisberg, J. M., Nice, D. J., & Taylor, J. H. 2010, ApJ, 722, 1030 (WNT)
- You, X. P., Hobbs, G., Coles, W. A., et al. 2007, MNRAS, 378, 493